Atg8 regulates vacuolar membrane dynamics in a lipidation-independent manner in *Pichia pastoris*

Naoki Tamura[1], Masahide Oku[1] and Yasuyoshi Sakai[1,2,*]

[1]Division of Applied Life Sciences, Graduate School of Agriculture, Kyoto University, Kitashirakawa-Oiwake, Sakyo, Kyoto 606-8502, Japan
[2]CREST, Japan Science and Technology Agency, 5, Chiyoda-ku, Tokyo 102-0075, Japan
*Author for correspondence (ysakai@kais.kyoto-u.ac.jp)

Accepted 26 August 2010
Journal of Cell Science 123, 4107-4116

doi:10.1242/jcs.070045

Summary

Atg8 is a ubiquitin-like protein that is required, along with its lipidation system, for autophagy in all eukaryotic cells. The lipidated form of Atg8 is anchored on the autophagosomal membrane during autophagy. Here, we demonstrate a previously unknown role for Atg8 in vacuolar membrane dynamics. In the methylotrophic yeast *Pichia pastoris*, vacuoles were found to fuse to become a single spherical vacuole during adaptation from glucose- to methanol-containing medium. Atg8 is responsible for the vacuolar fusion in *P. pastoris* during this adaptation to methanol. Although vacuole fusion required processing of Atg8 at the C-terminus, it did not require lipidation of Atg8 for autophagy. This is the first report of the function of any Atg8 protein family member in a process other than autophagy that is independent of lipidation.

Key words: Vacuole, Autophagy, Membrane fusion

Introduction

Autophagy is one of the major pathways of protein degradation. Molecular studies of autophagy have revealed that it is a highly conserved process in lower to higher eukaryotes accomplished through common molecular processes by the autophagy-related (Atg) proteins (Klionsky et al., 2003). During the autophagic process, double membrane structures called autophagosomes are formed to sequester intracellular components such as organelles and proteins, and they are transported into the vacuole or lysosome for complete degradation.

Atg8 is a core conserved Atg molecule that is necessary for autophagy. During autophagy, Atg8 (or the mammalian homolog LC3) localizes to autophagosomal membranes, and its expression is induced upon the induction of autophagy, such as occurs during nutrient starvation (Huang et al., 2000; Kirisako et al., 1999). Atg8 is lipidated by two ubiquitin-like systems (Ichimura et al., 2000; Kirisako et al., 2000; Mizushima et al., 1998) where Atg4 protease removes the C-terminus of Atg8 to expose a glycine residue, whereupon the cleaved Atg8 is recognized and activated by Atg7 (E1) through the exposed glycine residue, and transferred to Atg3 (E2). Finally, the exposed glycine residue of Atg8 is covalently conjugated to phosphatidylethanolamine (PE) (Ichimura et al., 2000; Oh-oka et al., 2008). Whereas this conjugation system has been reconstituted in vitro (Ichimura et al., 2004), complete conjugation in vivo requires the Atg5–Atg12–Atg16 complex (Kuma et al., 2002; Mizushima et al., 1998), which is formed through another ubiquitin-like system, involving Atg7 and Atg10. Recently, this complex was shown to function as an E3-like enzyme during Atg8 lipidation (Fujita et al., 2008; Hanada et al., 2007). Additionally, Nakatogawa and co-workers reported the ability of Atg8 to mediate membrane-tethering and hemifusion in *Saccharomyces cerevisiae* in vitro (Nakatogawa et al., 2007). Although Atg8 was originally characterized as a microtubule-associated protein (Lang et al., 1998) and has been well studied as part of the machinery for autophagy, involvement of Atg8 in other biological processes is not known.

The yeast vacuole is a model organelle that has been studied to gain a better understanding of membrane dynamics, including homotypic membrane fusion (Efe et al., 2005; Weisman, 2003; Wickner and Haas, 2000). In *S. cerevisiae*, homotypic vacuolar fusion has a crucial role in vacuolar inheritance and adaptation to hypo-osmotic stress (Efe et al., 2005; Weisman, 2003; Wickner and Haas, 2000).

Here we report a new role for Atg8 in the methylotrophic yeast *Pichia pastoris* in homotypic vacuolar fusion, which occurs in an autophagy-independent manner. Depletion of *P. pastoris* Atg8 leads to impairment of vacuolar inheritance. Surprisingly, Atg8 lipidation is not required for these functions, unlike autophagy activity. To our knowledge, this is the first demonstration of a physiological role for Atg8 in cellular events other than autophagy.

Results

Deletion of *ATG8* results in abnormal vacuolar shape

P. pastoris can use methanol as the sole carbon and energy source. Adaptation of glucose-grown *P. pastoris* cells to methanol medium leads to a great increase in the number and size of peroxisomes (van der Klei et al., 2006). In this study, we observed a morphological change in the vacuole during the methanol adaptation period. A wild-type strain shifted to methanol medium for 2 hours contained a single spherical vacuole per cell, compared with 2–4 clustered vacuoles per cell when growing on glucose medium (Fig. 1A).

To examine the morphological change after methanol adaptation of *P. pastoris* in greater detail, we performed a morphometric analysis during the transition process by counting the cells exhibiting a single spherical vacuole over time (Fig. 1B). FM4-64-labeled *P. pastoris* cells under methanol adaptation were sampled, and fluorescence images were immediately taken. It was found that the number of cells containing a single round vacuole increased immediately following the shift to methanol medium, and the

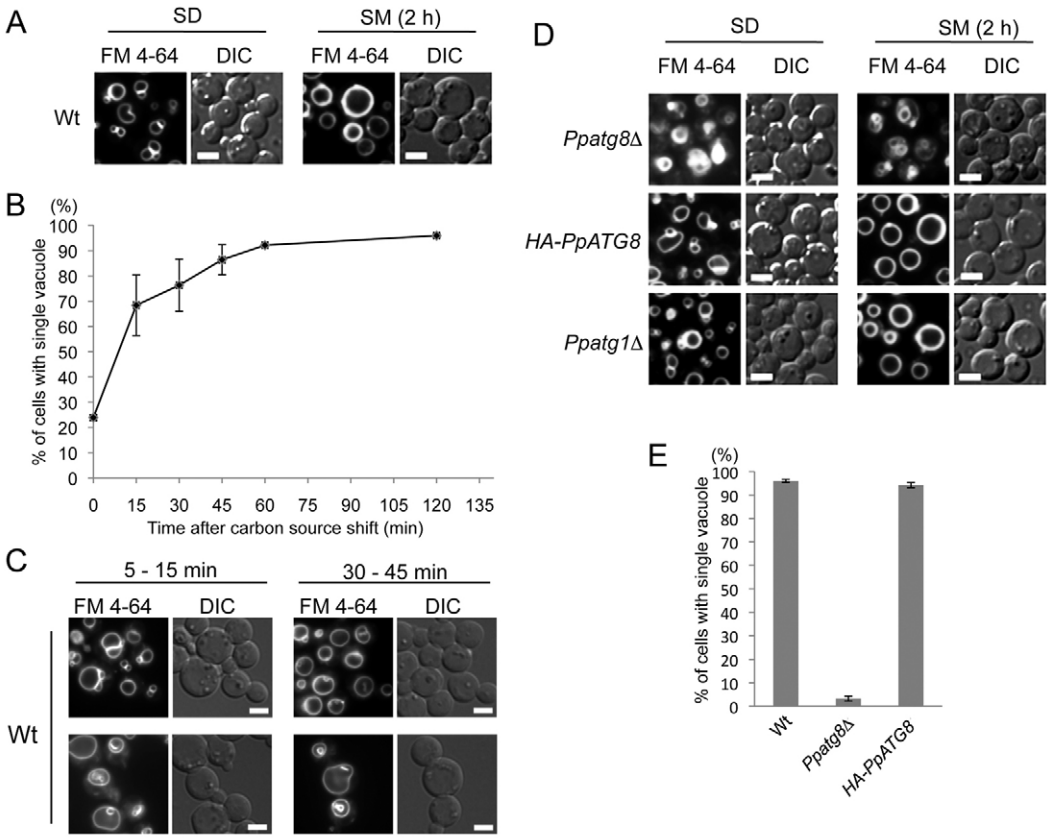

Fig. 1. *P. pastoris* Atg8 regulates vacuolar shape in an autophagy-independent manner. (**A**) Morphological analysis of vacuoles in wild-type *P. pastoris* under fluorescence microscopy. Vacuoles were stained with FM 4-64. After 1 to 2 hours of methanol adaptation, vacuoles fused to form a single spherical vacuole. (**B**) Time course of vacuolar dynamics during methanol adaptation. The graph shows the percentage (%) of cells from each strain that contained a single spherical vacuole after 2 hours of methanol adaptation. (**C**) Intermediate vacuolar structures detected during methanol adaptation. The boundary region of the vacuolar membranes was observed to be pinched off at the vertex site, and released into the vacuolar lumen. (**D**) Morphological analysis of vacuoles in *P. pastoris* mutant strains under fluorescence microscopy. Although cells of the *atg1*Δ strain contained a single vacuole similar to that observed in the wild-type strain, cells of the *atg8*Δ strain contained a vacuole of abnormal shape. PpAtg8 expression in the *atg8*Δ strain restores normal vacuolar shape. Images are shown for the *Ppatg8*Δ strain, HA–Atg8 (cells of the *Ppatg8*Δ strain ectopically expressing *HA-Atg8*) and *Ppatg1*Δ strain. (**E**) The percentage of cells of the indicated strains containing a single spherical vacuole after 2 hours of methanol adaptation. The error bars represent s.d. of the results from three independent experiments. Scale bars: 1 μm.

percentage of cells containing a single rounded vacuole reached more than 90% of the total cells after 1 hour, and remained the same after 2 hours.

During homotypic vacuolar fusion, three distinct microdomains are identifiable: the boundary region, the outside edge and the vertex site (Wang et al., 2002). Vacuolar homotypic fusion was postulated to occur at the vertex site, resulting in fission with the release of boundary regions into the vacuolar lumen to complete fusion (Wang et al., 2003; Wang et al., 2002).

During morphological analysis after methanol adaptation, we observed some cells in which the boundary regions of the clustered vacuoles had just been pinched off and were released into the lumen (Fig. 1C). This fusion event could also be followed under a fluorescence microscope with kinetics comparable with those of the morphometric experiment (Fig. 1B; supplementary material Movie 1). In this movie, the boundary membranes stained with FM 4-64 were successively released into the vacuolar lumen, and then they disappeared. These results are consistent with the observation that vacuolar fusion occurred at the vertex sites between neighboring vacuoles and that the boundary membranes were degraded in the vacuolar lumen.

In contrast to the spherical vacuoles observed in wild-type cells, methanol-induced cells of the *Ppatg8*Δ strain exhibited an abnormal vacuolar shape and did not form a single rounded vacuole after 2 hours of methanol adaptation (Mukaiyama et al., 2004). The *Ppatg8*Δ cells exhibited inefficient and unequal FM 4-64 staining of vacuoles, and vacuoles in glucose-grown cells also had an unusual shape, in which normal lobe-like vacuolar structures of the wild-type strain were not observed (Fig. 1D). Expression of an HA-tagged Atg8 in the *Ppatg8*Δ strain restored the spherical shape of the vacuole. Most of the other tested mutants (*Ppatg1*Δ, *Ppatg2*Δ, *Ppatg7*Δ, *Ppatg9*Δ, *Ppatg11*Δ, *Ppatg16*Δ, *Ppatg17*Δ, *Ppatg18*Δ, *Ppatg26*Δ) except *Ppatg4*Δ (see below) and *Ppatg24*Δ (Ano et al., 2005) contained a single spherical vacuole after a 2 hour methanol adaptation, which was similar to that observed in the wild-type strain (Fig. 1D).

We next calculated the percentage of cells containing a single vacuole from the wild-type and *Ppatg8*Δ strains, along with those of the *Ppatg8*Δ strain that had been complemented by expression of HA-*PpATG8*, over a period of 2 hours following induction of methanol adaptation (Fig. 1E). After a 2 hour methanol adaptation, most of the wild type, *Ppatg1*Δ and HA-*PpATG8*-complemented

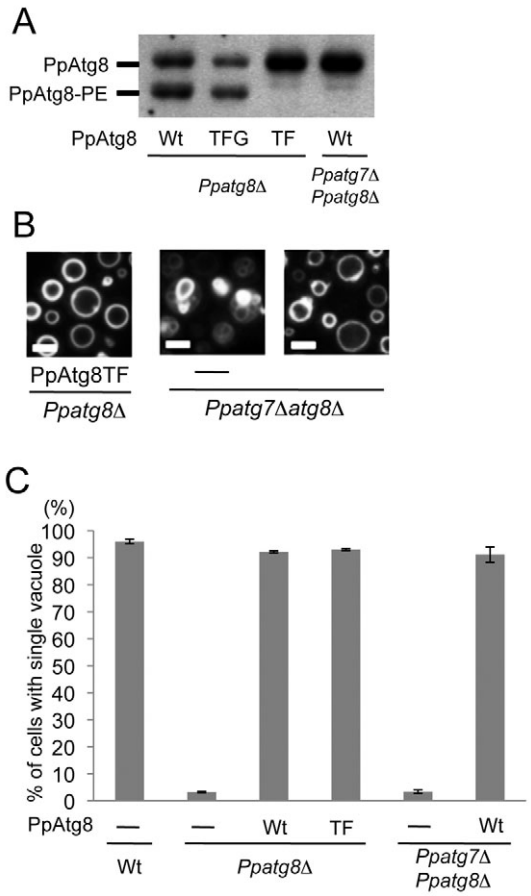

Fig. 2. Lipidation of *P. pastoris* Atg8 is dispensable for the maintenance of vacuolar shape. (**A**) Lipidation of HA–Atg8 variants in *Pichia* mutant strains. Lipidated and non-lipidated forms of HA–Atg8 were separated by urea-SDS-PAGE as previously described (Mukaiyama et al., 2004) and detected by immunoblot analysis. The TFG and TF mutants of Atg8 are defined in Table 1. Cells were grown in methanol medium for 12 hours, collected, and analyzed. (**B**) Morphological analysis of vacuoles under fluorescence microscopy. The vacuoles were stained with FM 4-64 in glucose medium (SD), and adapted in methanol medium (SM) for 2 hours. Scale bars: 1 μm. (**C**) The percentage of cells of the indicated strains containing a single spherical vacuole after 2 hours of methanol adaptation. The error bars represent the s.d. of the results from three independent experiments.

cells contained a single spherical vacuole, whereas cells of the *Ppatg8*Δ strain exhibited abnormal vacuoles throughout the observation period. These data suggest that PpAtg8 has a crucial role in the regulation of vacuolar shape during methanol adaptation, in a manner that is independent of the autophagic process.

Lipidation is not required for the regulation of vacuolar shape

Atg7 functions as an E1 enzyme in ubiquitin-like conjugation systems during autophagy, both the lipidation of Atg8 and the formation of the Atg5–Atg12 complex. We therefore examined whether lipidation is required for the maintenance of normal vacuolar shape in the *Ppatg7*Δ strain. We were unable to detect lipidated Atg8 (Atg8–PE), which migrates with greater mobility than non-conjugated Atg8 during urea-SDS-PAGE, in the *Ppatg7*Δ strain (Fig. 2A) (Mukaiyama et al., 2004). After 2 hours of methanol adaptation, we observed a single spherical vacuole in the *Ppatg7*Δ strain, as observed in the wild-type and *Ppatg1*Δ strains (Fig. 2B).

Table 1. *Pichia pastoris* Atg8 derivatives

Designation	C-terminal sequence
Atg8	TFG ! DIPGVEEIE*
Atg8 TFG	TFG*
Atg8 TF	TF*
Atg8 G116A	TFADIPGVEEIE*
Atg8 TFA9	TFAAAAAAAAA*

In Atg8, ! and * represent the *P. pastoris* Atg4 cleavage site and the C terminus, respectively.

Lipidation of Atg8 occurs through conjugation with the Gly116 residue of Atg8 (Mukaiyama et al., 2004). We next examined whether the Gly116 residue of Atg8 is necessary for the maintenance of vacuolar shape. To test this, we first expressed in the *Ppatg8*Δ strain, mutant Atg8 proteins that had been truncated at the C-terminal region, such that they either retained (Atg8 TFG) or lacked (Atg8 TF) this key glycine residue (Table 1), respectively. By urea-SDS-PAGE, we confirmed that the Atg8 TF protein was not conjugated to lipid as efficiently as the wild-type Atg8 in the *Ppatg7*Δ cells. However, Atg8 TFG was normally lipidated (Fig. 2A). Notably, a similar percentage of cells expressing the Atg8 TF protein contained a single spherical vacuole, similarly to the wild-type cells (Fig. 2B,C). These results indicate that lipidation of Atg8 is not required for the regulation of vacuolar shape.

Atg8 associates with vacuoles in a lipidation-independent manner

As shown in Figs 1 and 2, Atg8 regulates vacuolar shape independently of its lipidation. Therefore, we next examined the intracellular localization of Atg8. A YFP–Atg8 expression plasmid was introduced into both the *Ppatg8*Δ and the *Ppatg7*Δ*atg8*Δ strains. The cells were grown to mid-log phase in SD medium and shifted to methanol medium for 1 hour. In the *Ppatg8*Δ strain, YFP–PpAtg8 localized to the vacuolar membrane and was observed to be enriched at vertex sites within the clustered vacuoles (Fig. 3A). In the double-knockout strain *Ppatg7*Δ*atg8*Δ strain, YFP–Atg8 continued to localize to the vacuolar membrane (Fig. 3A), although there was a decrease in the level of vacuolar localization of YFP–Atg8 in this strain. Association of YFP–Atg8 to the vacuolar membrane was also found with confocal microscopy (supplementary material Fig. S1).

To confirm that the membrane-associated localization of Atg8 is independent of its lipidation, we performed a subcellular fractionation analysis on *Ppatg7*Δ*atg8*Δ cells expressing HA-tagged Atg8. These cells were grown in SD medium, shifted to methanol medium for 30 minutes and subjected to differential centrifugation. Although HA–Atg8 was mainly detected in the high-speed supernatant (HSS) fraction containing the cytosol, a significant fraction was detected in the low-speed pellet (LSP) fraction, which contained the vacuole (see below). By contrast, the cytosolic marker protein Pgk1 was exclusively detected in the HSS fraction, providing a cytosolic control for this subcellular fractionation experiment (Fig. 3B).

Membrane association of the non-lipidated form of Atg8 was also supported by fractionation experiments with the *Pichia* strain expressing HA–Atg8 TF and a vacuolar membrane marker Vac8–YFP (supplementary material Fig. S2). This experiment showed that Vac8–YFP was enriched in the LSP fraction. Independently,

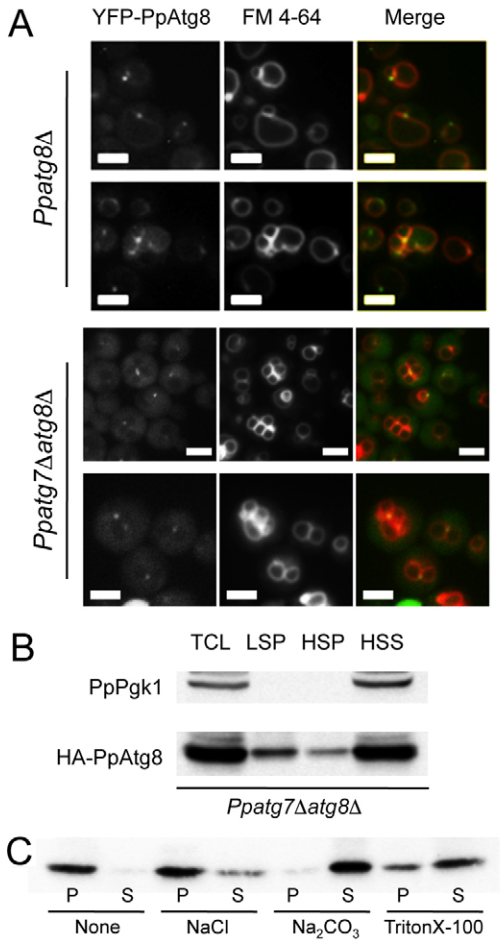

Fig. 3. YFP–Atg8 associates with the vacuoles in a lipidation-independent manner. (**A**) YFP-tagged Atg8 was introduced into the *Ppatg8*Δ and *Ppatg7*Δ*atg8*Δ strains. Vacuoles were stained with FM 4-64 and shifted to methanol medium for 1 hour. Samples were analyzed by fluorescence microscopy. Scale bars: 1 μm. (**B**) Subcellular fractionation analysis of HA–Atg8 in the *Ppatg7*Δ strain. Cells were shifted to methanol medium for 30 minutes and lysed with a Dounce homogenizer to generate total cell lysates (TCL). The TCL was centrifuged at 13,000 ***g***, and the resultant pellet fraction (LSP) and supernatant fraction (LSS) were obtained. Subsequently, the obtained LSS was centrifuged at 100,000 ***g*** to generate the high-speed pellet (HSP) and high-speed supernatant (HSS) fractions. These fractions were subjected to immunoblot analyses. The blot was probed with anti-Pgk1 and anti-HA. Pgk1 is a cytosolic marker protein. (**C**) Biochemical characterization. The LSP fraction was treated with 1 M NaCl, 100 mM Na_2CO_3, pH 11.5, or 1% Triton X-100, and centrifuged again at 13,000 ***g***. The resultant pellet and supernatant fractions were analyzed by immunoblot analysis using anti-HA.

vacuoles were purified from the same strain by the flotation method. Although HA–Atg8 TF was associated with the floating light-density fraction (FLF: the putative vacuole-enriched fraction), the cytosolic marker Pgk1 was not (supplementary material Fig. S2B).

To determine how soluble Atg8 is able to associate with membranes, the LSP membrane fraction (Fig. 3B) was subjected to further biochemical analysis. The LSP was treated with either 1 M NaCl, 150 mM Na_2CO_3 (pH 11.5), or 1% Triton X-100 for 15 minutes on ice, and centrifuged again at 13,000 ***g***. Treatment of the LSP fraction with either Na_2CO_3 or Triton X-100 led to solubilization of HA–Atg8 (Fig. 3C). From these results, it appears that a fraction of the non-lipidated Atg8 protein is peripherally associated with the vacuolar membrane.

The function of Atg8 in maintenance of vacuolar shape is correlated with its membrane tethering and hemifusion activity

Nakatogawa and colleagues reported that *S. cerevisiae* Atg8 anchored to liposomes via an Atg7 and Atg3 conjugation reaction was able to mediate tethering and hemifusion in vitro (Nakatogawa et al., 2007). They further isolated various Atg8 mutant alleles defective in autophagy, and classified them into three groups depending on the levels of non-lipidated Atg8 under starvation conditions. For the Class I mutants, the levels of the non-lipidated forms were similar to that of the wild type. However, compared with the wild type, lower levels of the non-lipidated forms were detected in the Class II mutants, whereas a larger amount of the non-lipidated Class III mutant accumulated. Although Class II and Class III mutants lost the tethering and hemifusion activities, Class I mutants were unaffected (Nakatogawa et al., 2007). Thus, we next examined whether the corresponding mutations introduced into *P. pastoris* Atg8 affected the maintenance of vacuolar shape. We expressed wild-type Atg8 or the mutant Atg8 protein each corresponding to Class I (K48, L50), Class II (I32, F104, Y106), or Class III (R65) mutant, in the *Ppatg8*Δ strain. We first evaluated the autophagic activities of these mutant proteins by monitoring their effect upon pexophagy, the autophagic degradation of peroxisomes (Sakai et al., 1998). We observed that all Class I, Class II and Class III Atg8 mutants lost pexophagy activity (data not shown). We next observed vacuoles in cells expressing these Atg8 mutants by fluorescence microscopy. Interestingly, although expression of Class II mutants (I32A, F104A, and Y106A) and a Class III mutant (R65A) did not restore normal vacuolar shape, expression of Class I mutants (K48A and L50A) and a control non-relevant mutant (V61A) did restore normal vacuolar shape (Fig. 4A,B). Expression of the Atg8 mutants in the *Ppatg7*Δ*atg8*Δ strain led to similar effects upon vacuolar shape as observed in the *Ppatg8*Δ strain (data not shown).

Biochemical analysis of these Atg8 variants indicated that Class I and Class III mutants were processed normally by Atg4 and that the expression of the conjugated form of Class II Atg8 mutants was reduced (Fig. 4C). To show that the defect of Class II mutants on vacuolar shape is not caused by the decreased amounts of the Atg8 proteins, Class II mutants (F104A) were introduced into the truncated variant of Atg8 with G116 at its C-terminus (Atg8–TFG, TFG). The mutated Atg8 TFG proteins were expressed from a plasmid that contained a strong *GAPDH* promoter, giving rise to levels of the mutant proteins that were equal to the level in the wild-type Atg8 (supplementary material Fig. S3A). However, expression of these mutants did not restore normal vacuolar shape to the *Ppatg7*Δ*atg8*Δ strain (supplementary material Fig. S3B,C), demonstrating that the tethering and hemifusion activity of Atg8 is essential for the maintenance of vacuolar shape.

Fluorescence microscopy of YFP-tagged Atg8 mutants suggested that all of these mutants colocalized with the vacuolar membrane (Fig. 4D). And localization of these YFP-tagged Atg8 mutants to the vacuolar membrane was also supported by subcellular fractionation experiments (Fig. 4E). These suggested that these Atg8 mutants were recruited to the vacuolar surface similarly to the wild-type protein. Thus, it is assumed that the mutations directly affect the ability of Atg8 to mediate fusion of the vacuolar membrane.

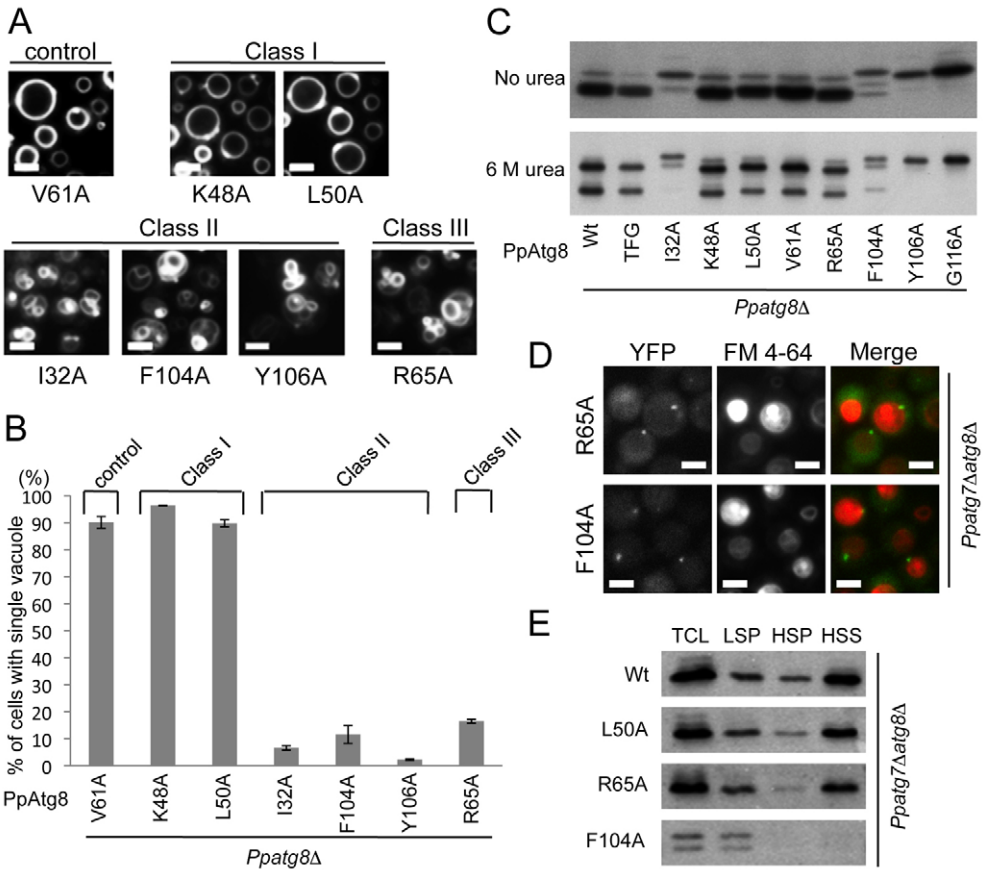

Fig. 4. The function of Atg8 in the maintenance of vacuolar shape is correlated with its ability to mediate membrane tethering and hemifusion. (**A**) Morphological analysis of vacuoles in tethering- and hemifusion-deficient strains by fluorescence microscopy. Class I mutants, K48A and L50A. Class II mutants, I32A, F104A and Y106A. Class III mutant, R65A. Cells were induced in methanol medium for 2 hours. (**B**) The percentage of cells containing a single spherical vacuole after 2 hours of methanol adaptation. The error bars represent the s.d. of the results from three independent experiments. (**C**) Biochemical analysis of HA–Atg8 mutant proteins. Samples were subjected to SDS-PAGE in the presence or absence of 6 M urea, and the HA–Atg8 variants were detected with anti-HA. (**D**) Intracellular localization of Atg8 F104A (class II) and Atg8 R65A (class III) mutants. Cells expressing YFP–Atg8 variants were grown in methanol medium for 1 hour, and their localizations were observed. (**E**) Subcellular fractionation analysis of Atg8 mutants in the *Ppatg7*Δ strain. Scale bars: 1 μm.

The removal of the C-terminal region is required for function of Atg8 in the maintenance of vacuolar shape

P. pastoris Atg8 possesses an additional nine amino acid residues at its C-terminus that are not present in *S. cerevisiae* Atg8 and which are cleaved off by the action of Atg4 (Table 2). We next examined whether retention of the C-terminal peptide affects the activity of Atg8 in the maintenance of vacuolar shape. As previously reported, Atg4 removes the C-terminal portion of Atg8, which was confirmed by SDS-PAGE (Mukaiyama et al., 2004) (supplementary material Fig. S4A). The *Ppatg4*Δ mutant exhibited abnormal vacuolar shape (supplementary material Fig. S4B,C), suggesting that the cleavage of the C-terminal peptide is necessary for Atg8 function in the maintenance of vacuolar shape.

This result was confirmed by the observation of abnormal vacuolar shape following expression of the processing-defective Atg8 variant, Atg8 G116A, in the *Ppatg8*Δ strain. Retention of the C-terminal peptide did not affect the localization of Atg8, as judged by fluorescence microscopy of cells expressing YFP–Atg8 G116A (supplementary material Fig. S4D) and by subcellular fractionation experiments (supplementary material Fig. S4E). Taken together, we conclude that the nine C-terminal amino acids of Atg8 need to be cleaved by Atg4 for the maintenance of vacuolar shape in *P. pastoris*.

Next, we substituted the amino acid residues of the C-terminal peptide with a stretch of nine alanine residues (Table 1). Expression of this Atg8 TFA9 mutant in the *Ppatg4*Δ*atg8*Δ strain restored normal vacuolar shape (supplementary material Fig. S2B,C). This result suggested that the original cleaved amino acid sequence, but not the polyalanine sequence, inhibited the catalytic activity of Atg8 in vivo. By contrast, the Atg8 TFA9 mutant could not recover the pexophagy defect (data not shown).

Deletion of *ATG8* causes severe growth defects on methanol

Previously, we showed that depletion of Atg8 impairs cell growth in methanol medium (Mukaiyama et al., 2002). We also reported that when *Pichia* cells were shifted from synthetic glucose medium to synthetic methanol medium, a type of autophagic pathway called lag-phase autophagy, is induced, which enables the cells to promptly exit from the lag phase (Yamashita et al., 2009). To assess whether the growth defect observed in the *Ppatg8*Δ strain was caused solely by the inability to induce lag-phase autophagy, we compared the growth profiles of the *Ppatg1*Δ, *Ppatg8*Δ and *Ppatg1*Δ*atg8*Δ double-knockout strains during methanol adaptation. We observed

Table 2. Negatively charged amino acid residues found in fungal Atg8 C-terminal peptides

Species	C-terminal sequence
Pichia pastoris	TFG ! **D**IPGV**EE**I**E***
Candida boidinii	TFG ! **DI**EGV**EE**ITDLD*
Hansenula polymorpha	TFG ! QL**E**GV**EE**TL*
Magnaporthe oryzae	TFG ! DLF**EE**V**E***
Chlamydomonas incerta	TFG ! GCGV**EE**LQ*
Schizosaccharomyces pombe	TFG ! TVFPF*
Saccharomyces cerevisiae	TFG ! R*

The symbols ! and * represent the Atg4 cleavage site and the C terminus, respectively.

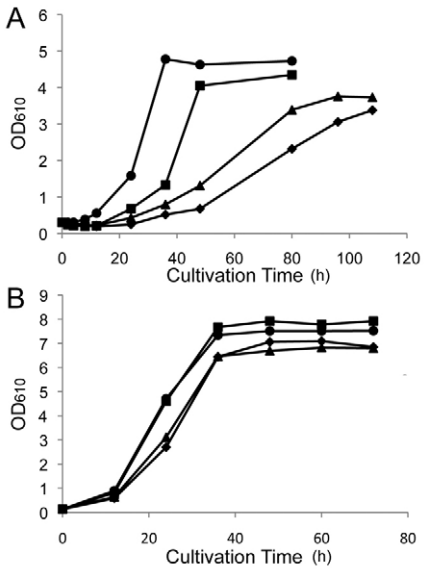

Fig. 5. Atg8 is required for optimal growth in methanol medium independent of autophagic function. (**A**) Growth in methanol medium (SM). (**B**) Growth in SM medium supplemented with 20 amino acids. ●, wild-type strain; ▲, *Ppatg8*Δ; ■, *Ppatg1*Δ; ◆, *Ppatg1*Δ *atg8*Δ strain.

that the *Ppatg8*Δ strain exhibited a more severe growth defect than the *Ppatg1*Δ strain (Fig. 5A). Furthermore, the *Ppatg1*Δ*atg8*Δ double-knockout strain exhibited slower growth than either of the single-knockout *Ppatg1*Δ or *Ppatg8*Δ strains. Although the differences in the growth on methanol medium among these mutants were small, they were reproducible (Yamashita et al., 2009). It has previously been reported that when an amino acid mixture or yeast extract is added to the synthetic methanol (SM) medium, the growth defect caused by lag phase autophagy is suppressed in other autophagy-deficient mutants, e.g. *Ppatg1*Δ and *Ppatg17*Δ (Yamashita et al., 2009). Therefore, *Ppatg8*Δ cells were shifted to methanol medium supplemented with amino acids to confirm that the slow growth of the *Ppatg8*Δ strain was not solely attributed to the defect in lag-phase autophagy. As expected, the *Ppatg8*Δ and *Ppatg1*Δ*atg8*Δ cells showed a growth defect even in the presence of amino-acid-supplemented medium, whereas the *Ppatg1*Δ cells grew at a similar rate to that of the wild-type strain (Fig. 5B). These results suggested that Atg8 has another physiological role in addition to autophagy during methanol adaptation, probably in the regulation of vacuolar shape.

Function of Atg8 during adaptation to hypo-osmotic stress and vacuole inheritance

In *S. cerevisiae*, vacuoles are known to change their shape upon osmotic change and during their inheritance. We next asked whether Atg8 is involved in these processes in *P. pastoris*. Wild-type, *Ppatg8*Δ and *Ppatg1*Δ strains were grown on SD medium with FM 4-64, collected, subjected to hypo-osmotic stress by resuspension in distilled water, and observed by fluorescence microscopy. The wild-type cells harbored a single round vacuole after hypo-osmotic stress that was similar to those observed in methanol-grown cells. By contrast, most *Ppatg8*Δ cells, which are deficient in vacuolar shape during methanol shift, failed to exhibit a significant change in the vacuolar shape (Fig. 6A,B). Although Atg8 and Atg8 TF protein could complement this vacuolar defect after hypo-osmotic stress in *Ppatg8*Δ cells, Atg8 G116A protein could not. This indicated that lipidation of Atg8, but not its C-terminal processing by Atg4, is dispensable for homotypic vacuolar fusion during adaptation to hypo-osmotic stress.

The vacuolar shape in the *S. cerevisiae atg8*Δ (*Scatg8*Δ) strain was also observed after its adaptation to hypo-osmotic adaptation after 2 hours, by counting the percentage of the cells containing a single rounded vacuole (supplementary material Fig. S5). More than 90% of the wild-type, *Scatg1*Δ, and *Scatg7*Δ cells had a single rounded vacuole after only 5 minutes of hypo-osmotic adaptation and remained the same at least for 2 hours; by contrast, only ~70% of the *Scatg8*Δ cells had a single rounded vacuole after 2 hours of hypo-osmotic adaptation. Therefore, the knockout effect of Atg8 on the vacuolar morphology is only partial in *S. cerevisiae*.

The vacuolar inheritance (*vac*) phenotype was indicated by the reduced number of inherited vacuoles (which had been pre-labeled with FM 4-64 in the mother cells) in daughter cells (supplementary material Fig. S6) (Weisman, 2003). Although more than 80% of the *P. pastoris* wild-type daughter cells possessed FM4-64-labeled vacuoles inherited from mother cells, less than 20% of *Ppatg8*Δ cells harbored the labeled vacuoles (supplementary material Fig. S6A,B). Similarly to the results from the methanol adaptation period, more than 70% of the daughter cells of the *Ppatg1*Δ strain and cells expressing the lipidation-deficient Atg8 TF mutant contained FM4-64-labeled vacuoles. By contrast, less than 20% of the daughter cells of the *Ppatg8*Δ strain expressing the processing-deficient Atg8 G116A mutant contained FM4-64-labeled vacuoles.

These results indicate that Atg8 in *P. pastoris* is responsible for the maintenance of vacuolar shape during hypo-osmotic adaptation and during vacuolar inheritance in an autophagy-independent manner, and that this type of regulation by Atg8 is partially conserved in *S. cerevisiae*.

Discussion

Lipidation of Atg8, but not its C-terminal processing by Atg4, is dispensable for the regulation of vacuolar fusion

When *P. pastoris* cells are shifted from glucose to methanol medium, their intracellular organelles, i.e. peroxisomes and vacuoles, undergo significant morphological change. In this study, we investigated the Atg8-dependent dynamics of changes in vacuolar shape during methanol adaptation.

A major finding in this study is that the lipidation of Atg8 is dispensable for the regulation of vacuolar shape. Neither Atg7, an E1-like enzyme of the Atg8-lipidation system, nor the Gly116 residue of Atg8 was necessary for this process. To our knowledge, this is the first description of a function of an Atg8 family protein that does not require lipidation. Consistently, Atg8 localized to the vacuolar membrane in a lipidation-independent manner in the *Ppatg7*Δ strain. Subsequent biochemical analysis of the *Ppatg7*Δ strain also indicated peripheral association of Atg8 with the membrane fraction. Vacuolar soluble NEM-sensitive factor attachment protein receptors (SNAREs) are reported to be enriched at vertex sites (Wang et al., 2003) and co-immunoprecipitated with *S. cerevisiae* Atg8 (Legesse-Miller et al., 2000). Thus it might be that Atg8 is involved in the vacuolar fusion together with other components of the fusion machinery.

Although lipidation of Atg8 was not required for the regulation of vacuolar fusion, Atg4-catalyzed processing of the Atg8 C-terminal peptide was required. The C-terminal peptide sequence of Atg8 contains a WEEL-motif-like sequence VEEI, and the replacement of this sequence with an alanine repeat sequence

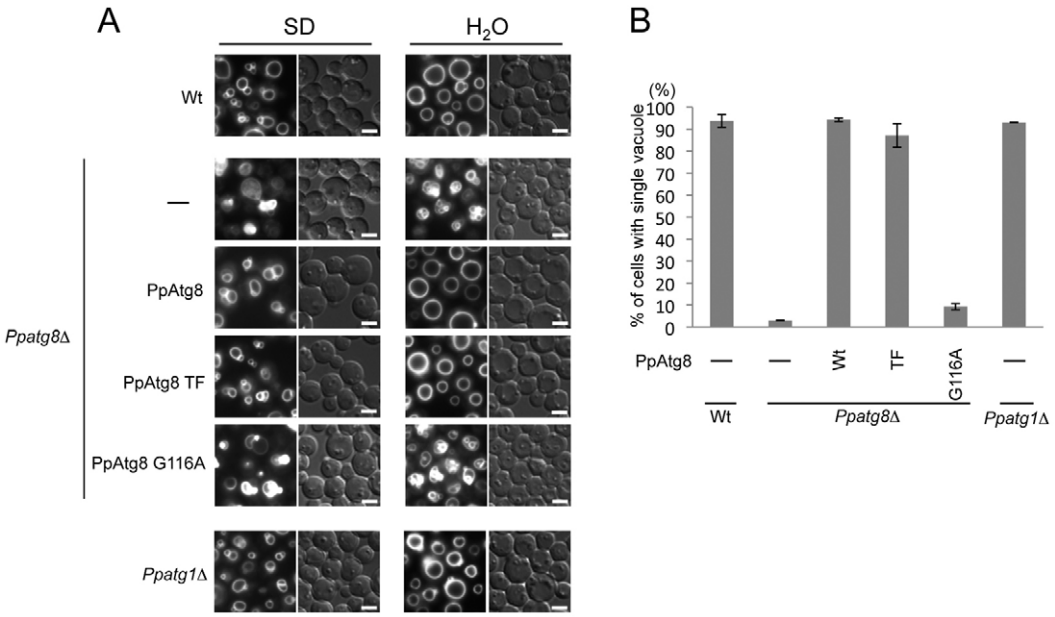

Fig. 6. Role of Atg8 in hypo-osmotic adaptation. (**A**) Vacuolar shape of *P. pastoris* under hypo-osmotic conditions. Cells were grown in glucose medium (SD) to mid-log phase, shifted to distilled water, and incubated for 2 hours. Scale bars: 1 μm. (**B**) The percentage of cells containing a single spherical vacuole after 2 hours of hypo-osmotic adaptation. The error bars represent the s.d. of the results from three independent experiments.

partially recovered its function in regulating vacuolar shape. Because the WEEL motif in *S. cerevisiae* Atg19 or mammalian p62 is known to function in the interactions with Atg8 or its homolog LC3 (Ichimura et al., 2008; Noda et al., 2008), the *P. pastoris* Atg8 C-terminal region might directly inhibit the catalytic activity of Atg8 in vivo. Atg8 proteins harboring such a WEEL-motif-like sequence are found in other methylotrophic yeasts, including *Hansenula polymorpha* and *Candida boidinii*, the plant pathogenic fungus *Magnaporthe oryzae*, and also in the green algae *Chlamydomonas incerta* (Table 2). However, because we could not detect an uncleaved form of the Atg8 protein in the *P. pastoris* wild-type strain, we do not know at this stage whether the processing of the C-terminus of Atg8 is involved in this regulatory function.

The function of Atg8 on the vacuolar membrane correlates with its tethering and hemifusion activity in vitro

Previously, *S. cerevisiae* Atg8 was shown to have membrane-tethering and hemifusion activity in vitro (Nakatogawa et al., 2007). In this study, we demonstrated that *P. pastoris* Atg8 mutants corresponding to those defective in catalytic tethering and hemifusion activity also lost the ability to promote the formation of a normal single spherical vacuole through a complete fusion reaction. Atg8 (or its LC3 homolog) has not been identified as a component of the vacuolar homotypic fusion machinery (Wickner and Haas, 2000), and *S. cerevisiae* Atg8 does not show complete fusion activity in vitro (Nakatogawa et al., 2007). Therefore, *P. pastoris* Atg8 is speculated to support the vacuolar fusion via its tethering and hemifusion activity. This idea is supported by the localization of Atg8 to the vacuolar membrane where fusion events actually occurred.

We found that Atg17–YFP, a marker protein for preautophagosomal structure (phagophore assembly site; PAS), colocalized with CFP–Atg8 at the vacuolar membrane (supplementary material Fig. S7). This observation might raise the argument that the vacuolar homotypic fusion observed here is indirect and mediated by heterotypic fusion between the vacuole and autophagosomes. However, (1) vacuolar fusion is observed in many *atg* mutants impaired in autophagosome formation, including the *Ppatg7*Δ strain; (2) vacuolar fusion is observed in a double-knockout *Ppatg11*Δ*atg17*Δ strain (Yamashita et al., 2009), in which basal key components for PAS organization are depleted (Cheong et al., 2008; Kawamata et al., 2008). From these, we think that Atg8 is directly involved in vacuolar homotypic fusion in *P. pastoris*.

Lipidation of Atg8 thorough a ubiquitin-like conjugation system is necessary for all autophagic processes. And its anchoring to the liposome membrane was necessary for hemi-fusion to occur in vitro. During methanol adaptation, Atg8 might be recruited to the vacuolar membrane through interaction with a molecule such as vacuolar SNARE, and facilitate complete fusion as if it is anchored to the membrane in its steric conformation. In *S. cerevisiae*, physical interaction of Atg8 with such molecules has been reported (Legesse-Miller et al., 2000).

Physiological roles of the maintenance of vacuolar shape by Atg8

The function of Atg8 in the regulation of vacuolar fusion is clearly distinct from that in autophagy. The core Atg proteins for all autophagic pathways, Atg1 and Atg7, and essential scaffold proteins for selective autophagy and non-selective pathways, Atg11 and Atg17, respectively, were dispensable for this process (data not shown), supporting an independent function of Atg8 in the regulation of vacuolar shape.

We believe that maintenance of vacuolar shape has an important role during methanol adaptation in a fashion that is independent of lag-phase autophagy (Yamashita et al., 2009). This is because: (1) the growth of the *Ppatg8*Δ strain was distinctively slower than that of the *Ppatg1*Δ strain, (2) the double-knockout *Ppatg1*Δ*atg8*Δ strain showed slower growth than the *Ppatg8*Δ strain, and (3) the

growth defect of the *Ppatg1*Δ strain was recovered fully by suppression of autophagy through supplementation with amino acids, whereas that of the *Ppatg8*Δ strain was not.

We found that both vacuolar fusion and lag-phase autophagy occurred under oleate-induced conditions and that both processes required Atg8 (data not shown). We observed severe growth inhibition on synthetic oleate-medium (both in the growth rate and growth yield) not only with the *Ppatg8*Δ strain but also with *Ppatg1*Δ, and *Ppatg1*Δ*atg8*Δ strains. Therefore, we speculate that the lack of lag-phase autophagy on oleate medium greatly affects growth on synthetic oleate medium.

We also compared the growth of the mutant strains on oleate medium in which lag-phase autophagy was suppressed by adding 0.5% yeast extract to the medium. Under these conditions, we could see some growth defect only with the *Ppatg8*Δ, and *Ppatg1*Δ*atg8*Δ strains, but not with the *Ppatg1*Δ strain (data not shown). The phenotypes of the *Ppatg8*Δ and *Ppatg1*Δ*atg8*Δ strains were similar but were less severe than those with methanol as shown in Fig. 5B. These results indicate that growth defects observed with both methanol and oleate complex media come not from an autophagy defect, but from a vacuolar morphology defect in the *Ppatg8*Δ strain.

We did not observe any growth defects with the *Ppatg1*Δ, *Ppatg8*Δ and *Ppatg1*Δ*atg8*Δ strains on glucose medium. The deficiency in the maintenance of vacuolar shape presumably causes a deficiency in the optimal growth on peroxisome-inducing carbon sources. The vacuoles surround the peroxisome clusters in methanol-induced cells of the *Ppatg8*Δ strain (Mukaiyama et al., 2004; Mukaiyama et al., 2002). This peculiar topology of the organelles might lead to sequestration of the peroxisomes from the cytosol, and might interfere with the efficient transfer of metabolites to and from the peroxisomes, the primary location of methanol metabolism. Another possible explanation could be the inefficient inheritance of vacuoles to daughter cells (required for lag-phase autophagy) during adaptation to methanol or oleate medium. At this stage, it remains to be seen whether the metabolic inhibition by vacuolar morphology or the inheritance defect is directly involved in the growth inhibition of the *Ppatg8*Δ strain on peroxisome-inducing carbon sources.

In the wild-type strains of *P. pastoris* and *S. cerevisiae* as well as the *Ppatg1*Δ, *Scatg1*Δ and *Scatg7*Δ strains, the vacuoles fused into a single organelle just after hypo-osmotic adaptation (10 minutes) and retained a single rounded shape for at least 24 hours of adaptation. Whereas the vacuoles in the *Ppatg8*Δ strain did not fuse to become a single rounded vacuole even after 24 hours of hypo-osmotic adaptation (data not shown), a considerable population (nearly 70%) of vacuoles in the *Scatg8*Δ strain could fuse to become a single rounded organelle after 2 hours (supplementary material Fig. S5). Furthermore, Atg8 was dispensable for vacuolar inheritance in *S. cerevisiae*, whereas its *P. pastoris* homolog was not (data not shown). Taken together, the contribution of Atg8 to the regulation of vacuolar shape in *S. cerevisiae* is less significant than that observed in *P. pastoris*.

In addition to functions during methanol adaptation and vacuolar inheritance, we believe that Atg8 activity is also crucial for the last stage of micropexophagy, at which time the fusion between the neighboring vacuoles in *P. pastoris* occurs in a lipidation-independent manner (Ano et al., 2005; Mukaiyama et al., 2004). During micropexophagy, Atg8 was observed to be localized at both the vacuoles and the micropexophagy-specific membrane apparatus (MIPA) (Mukaiyama et al., 2004) (data not shown). Therefore, Atg8 is speculated to regulate both the formation of MIPA in a lipidation-dependent manner and vacuolar fusion in a lipidation-independent manner. However, how Atg8 conducts such dual roles during micropexophagy remains to be determined.

Our present results firstly show that Atg8 might be involved in the process of vacuolar fusion, i.e., complete fusion in vivo. However, because *S. cerevisiae* Atg8 was previously shown to catalyze only the hemifusion reaction in vitro, it remains unclear which step of the reaction during macroautophagy is catalyzed by Atg8. Is Atg8 involved in the closure of the phagophore or the formation or extension of autophagosomes? The present results have raised another possibility that Atg8 is involved in a process of complete fusion at some point during the autophagic processes. Further molecular analyses on Atg8 family proteins will provide new insights into the regulation of membrane traffic in the cells.

Materials and Methods

Yeast strains, media and reagents

Supplementary material Table S1 describes the *P. pastoris* and *S. cerevisiae* strains used in this study. YPD (yeast extract, peptone, dextrose) medium consisted of 1% yeast extract, 2% bactopeptone, and 2% glucose. SD (synthetic dextrose) medium contained 0.67% yeast nitrogen base without amino acids, and 2% glucose, and SM (synthetic methanol) medium contained 0.67% yeast nitrogen base without amino acids and 0.8% methanol. These synthetic media were supplemented with the appropriate amino acids (100 μg/ml arginine, 100 μg/ml histidine) for auxotrophic strains. An anti-hemagglutinin (HA) mouse mAb (16B12) was purchased from Babco, and an anti-Pgk1 mouse mAb (22C5) was purchased from Molecular Probes. An anti-GFP mouse mAb (JL-8) was purchased from Molecular Probes. An anti-mouse IgG HRP conjugate was purchased from Millipore.

Plasmid construction

The oligonucleotide primers used for PCR reactions are listed in supplementary material Table S2. The plasmids used in this study are listed in supplementary material Table S3. The *PpATG8* promoter region, 3×HA, and the *PpATG8*ORF regions were amplified by primers ATG8PromFw-EcoRI and ATG8TFRv-XhoI using pHM104 as a template DNA, and the fragments were inserted into the *Eco*RI and *Xho*I sites of the expression vector pIB1 (Sears et al., 1998), and the resulting plasmid was designated pNT801. pNT802, pNT803, pNT804, pNT805, pNT806, pNT807 and pNT808 were derived from pHM104 by site-directed mutagenesis (Stratagene). The 3×HA and *PpATG8*ORF regions were amplified by primers HAFw-EcoRI and ATG8FGRv-XhoI using pHM104, pNT806, or pNT807 as templates, and then inserted into the *Eco*RI-*Xho*I site of the expression vector pIB2 (Sears et al., 1998), and the resulting plasmids were designated pNT809, pNT810 and pNT811, respectively. The *Spe*I-*Eco*RI fragment isolated from pSAP115 was inserted into the *Spe*I-*Eco*RI site of pHM110 (Mukaiyama et al., 2002), and the resulting plasmid was designated pNT812. pNT813, pNT814, and pNT815 were derived from pNT812 by site-directed mutagenesis (Stratagene). The *PpATG8* promoter region, 3×HA, and the *PpATG8*ORF regions were amplified using primers ATG8PromFw-EcoRI and ATG8A9Rv-XhoI using pHM104 as a template, and then inserted into the *Eco*RI-*Xho*I site of the expression vector pIB1 (Sears et al., 1998), and the resulting plasmid was designated pTM816. pNT817 was constructed using a primer set of CFPFw-PstI and CFPRv-PstI. pNT204 was newly constructed from pIB2 (Sears et al., 1998) by deleting the *GAPDH* promoter and by replacing the *PpHIS4* with *PpARG4*. pNT205 and pNI005 were constructed on pNT204 in a similar way using a primer set of YFPFw-HindIII and YFPRv-HindIII, and that of ATG17UPFw-BamHI and ATG17Rv-XhoI, respectively. These plasmids were introduced into *P. pastoris* cells following a standard protocol (Higgins and Cregg, 1998). Proper gene disruption was confirmed by Southern blot analysis, as described previously (Sakai et al., 1991). *S. cerevisiae atg* mutant strains were generated as previously described (Longtine et al., 1998).

Microscopic analyses following hypo-osmotic stress and during vacuole inheritance

P. pastoris cells were grown in 5 ml YPD medium to the stationary phase at 28°C, and transferred to 5 ml SD medium containing 0.93 mg/ml FM4-64 (Molecular Probes) to label the vacuolar membrane. Then, the cells were grown to mid-log phase at 28°C, and shifted to 5 ml of SM medium or 5 ml distilled water at 28°C. *S. cerevisiae* cells were grown in 5 ml YPD medium to the stationary phase at 28°C, and transferred to 5 ml YPD medium containing 0.93 mg/ml FM4-64 (Molecular Probes) to label the vacuolar membrane. Then, the cells were grown to mid-log phase at 28°C, and shifted to 5 ml distilled water at 28°C. Vacuole inheritance was assessed by staining the *P. pastoris* cells with FM 4-64 for 4 hours in 5 ml YPD, and shifted to SD without FM 4-64 for 5 hours.

Fluorescence microscopy was performed using an IX70 inverted microscope (Olympus) equipped with a Uplan Apo 100×/1.35 oil iris objective lens using mirror/filter units U-MWIG (Olympus) for FM 4-64, and UMF2 (Olympus) filter set (XF104-; Omega Optical) for YFP, or an IX81 (Olympus) equipped a Uplan Apo 100×/1.35 oil iris objective lens using XF104-3 filter set (Omega Optics) for YFP, and U-MRFPHQ unit (Olympus) for FM 4-64. Confocal microscopy was carried out using a Zeiss LSM510 META laser-scanning confocal microscope equipped with diode, argon, and Helium-Neon laser lines. Both YFP and FM 4-64 signals were acquired using a-plan FLUAR 100× lens (Zeiss) with pinhole setting to 1.02 Airy Units for YFP acquisition. For the time-lapse experiment, we used the ONIX Dynamic Cell Culture Platform (CELL ASIC). Image data were captured with charge-coupled device cameras SenSys (PhotoMetrics) for IX70 and DP30BW (Olympus) for IX80. These data were acquired and analyzed by using MetaMorph. 4.6 or 7.0, and saved as TIFF files. The TIFF image files were optimized for their contrast on Photoshop CS3 (Adobe).

Morphometric analysis

When cells were shifted to SM or distilled water, the ratio of the number of cells possessing a single spherical vacuole to the number of total counted cells was determined from the acquired images. At least 500 cells were counted for each time point, and the experiments were repeated at least three times. For assessment of vacuolar inheritance, the numbers of budding cells with or without the FM 4-64 signal in the nascent bud sites were counted in at least 200 budding cells. The data were collected from three independent experiments.

Immunoblot analysis

To prepare samples for immunoblot analyses, cells were grown in SD to A_{610}=1.0 and then shifted to SM for 12 hours. Cells were harvested, washed once with water, suspended in lysis buffer containing 50 mM Tris-HCl, pH 7.5, 1 mM EDTA, EDTA-free complete protease inhibitor cocktail (Roche Diagnostics), 1 mM PMSF and lysed by Multi-beads shocker (Yasui Kikai). The resulting cell extracts were centrifuged at 1000 ***g*** for 5 minutes at 4°C to generate cell lysates, and dissolved in SDS sample buffer (Yamashita et al., 2006). Samples containing 10 μg protein were loaded on 12% SDS-PAGE gels, and transferred to nitrocellulose membranes. To separate Atg8–PE from soluble Atg8, cell lysates were analyzed by SDS-PAGE on gels containing 6 M urea (urea-SDS-PAGE), and transferred to PVDF membranes. These blots were incubated with anti-HA or anti-Pgk1 (diluted 1:1000) in TBS-T buffer (3 g Tris, 8 g NaCl, 0.2 g KCl, 0.1% Tween 20, pH 8.0) for 1 hour and washed three times with TBS-T. Subsequently, blots were incubated with an anti-mouse IgG HRP (diluted 1:10000) in TBS-T for 1 hour, and washed four times in TBS-T. Immunoreactive bands were visualized with the Western Lightning Chemiluminescence Reagent Plus (Perkin-Elmer Life Science) and the signals were detected by Light-Capture II (ATTO).

Subcellular fractionation analysis

Cells for subcellular fractionation experiments were grown in 100 ml SD to A_{610}=1 and shifted to 100 ml SM medium for 30 minutes. Cells were then collected, and converted to spheroplasts in spheroplast buffer with 50 mM HEPES-KOH, pH 7.5, 1 M sorbitol, 0.3% (v/v) 2-mercaptoethanol, and 0.1 mg/ml zymolyase 100T (Seikagaku Kogyo). The spheroplasts were washed twice with 50 mM HEPES-KOH, pH 7.5 and 1 M sorbitol at 4°C, resuspended in lysis buffer containing 25 mM HEPES-KOH, pH 6.9, 0.2 M sorbitol, EDTA-free complete protease inhibitor cocktail (Roche), 1 μg/ml Pepstatin A, 1 mM PMSF, and 0.1 mM $MgCl_2$, and then gently lysed by Dounce homogenization. The lysed cells were centrifuged at 500 ***g*** twice, and the supernatant fraction was retrieved as total cell lysates (TCL). Each TCL fraction containing ~100 μg protein was centrifuged at 13,000 ***g*** for 20 minutes at 4°C to generate the low-speed pellet fraction (LSP) and the low-speed supernatant fraction (LSS). Subsequently, LSS were centrifuged at 100,000 ***g*** for 40 minutes at 4°C to obtain the high-speed pellet fraction (HSP) and the high-speed supernatant fraction (HSS). Each of the obtained fractions was precipitated by incubation with 10% TCA at 4°C overnight and suspended in the SDS sample buffer. The samples were analyzed by immunoblot using anti-HA or anti-Pgk1.

To evaluate the association of Atg8 with the membrane fraction, the LSP fraction was treated with 1 M NaCl in lysis buffer, 1% Triton X-100 in lysis buffer, or 100 mM Na_2CO_3 in water with 0.2 M sorbitol and 0.1 mM $MgCl_2$, and incubated for 20 minutes on ice. The reaction mixture was centrifuged at 13,000 *g* for 20 minutes at 4°C to yield pellet and supernatant fractions. These fractions were then TCA-precipitated and subjected to immunoblot analysis.

Vacuoles were isolated from *P. pastoris* by the flotation method (Conradt et al., 1992; Haas et al., 1994) with modification. The spheroplasts were broken in 10 mM HEPES-KOH, pH 6.9 with 0.2 M sorbitol, EDTA-free complete protease inhibitor cocktail, 1 μg/ml Pepstatin A, 0.1 mg/ml Pefablock (Roche), 0.1 mM $MgCl_2$, and 12% Ficoll (Nacalai Tesque) by Dounce homogenization. A buffer containing 10 mM HEPES-KOH, pH 6.9 with 0.2 M sorbitol, EDTA-free complete protease inhibitor cocktail, 1 μg/ml PepstatinA, 0.1 μg/ml Pefablock, 0.1 mM $MgCl_2$ and 8% Ficoll was used to overlay the lysates in a tube that was centrifuged at 100,000 ***g*** for 40 minutes at 4°C to obtain the light density fraction. The floating fraction was collected and subjected to immunoblot analysis. The blots were analyzed with anti-HA, anti-Pgk1 and anti-GFP.

Growth experiments

To exclude growth differences resulting from the differences in auxotrophic requirements, the strains used for growth experiments were derived by introducing the corresponding auxotrophic marker genes. Growth was determined as previously described (Yamashita et al., 2009).

This work was supported in part by a Grant-in-Aid for Scientific Research on Priority Areas 18076002, Grants-in-Aid for Scientific Research (B) 22380052, from the Ministry of Education, Culture, Sports, Science and Technology of Japan, and a CREST grant from the Science and Technology Agency of Japan, to Y.S.

Supplementary material available online at
http://jcs.biologists.org/cgi/content/full/123/23/4107/DC1

References

Ano, Y., Hattori, T., Oku, M., Mukaiyama, H., Baba, M., Ohsumi, Y., Kato, N. and Sakai, Y. (2005). A sorting nexin PpAtg24 regulates vacuolar membrane dynamics during pexophagy via binding to phosphatidylinositol-3-phosphate. *Mol. Biol. Cell* **16**, 446-457.

Cheong, H., Nair, U., Geng, J. and Klionsky, D. J. (2008). The Atg1 kinase complex is involved in the regulation of protein recruitment to initiate sequestering vesicle formation for nonspecific autophagy in Saccharomyces cerevisiae. *Mol. Biol. Cell* **19**, 668-681.

Conradt, B., Shaw, J., Vida, T., Emr, S. and Wickner, W. (1992). In vitro reactions of vacuole inheritance in Saccharomyces cerevisiae. *J. Cell Biol.* **119**, 1469-1479.

Efe, J. A., Botelho, R. J. and Emr, S. D. (2005). The Fab1 phosphatidylinositol kinase pathway in the regulation of vacuole morphology. *Curr. Opin. Cell Biol.* **17**, 402-408.

Fujita, N., Itoh, T., Omori, H., Fukuda, M., Noda, T. and Yoshimori, T. (2008). The Atg16L complex specifies the site of LC3 lipidation for membrane biogenesis in autophagy. *Mol. Biol. Cell* **19**, 2092-2100.

Haas, A., Conradt, B. and Wickner, W. (1994). G-protein ligands inhibit in vitro reactions of vacuole inheritance. *J. Cell Biol.* **126**, 87-97.

Hanada, T., Noda, N. N., Satomi, Y., Ichimura, Y., Fujioka, Y., Takao, T., Inagaki, F. and Ohsumi, Y. (2007). The Atg12-Atg5 conjugate has a novel E3-like activity for protein lipidation in autophagy. *J. Biol. Chem.* **282**, 37298-37302.

Higgins, D. R. and Cregg, J. M. (1998). *Pichia Protocols* (*Methods in Molecuolar Biology*), Vol. 103. Totawa, NJ: Humana Press.

Huang, W. P., Scott, S. V., Kim, J. and Klionsky, D. J. (2000). The itinerary of a vesicle component, Aut7p/Cvt5p, terminates in the yeast vacuole via the autophagy/Cvt pathways. *J. Biol. Chem.* **275**, 5845-5851.

Ichimura, Y., Kirisako, T., Takao, T., Satomi, Y., Shimonishi, Y., Ishihara, N., Mizushima, N., Tanida, I., Kominami, E., Ohsumi, M. et al. (2000). A ubiquitin-like system mediates protein lipidation. *Nature* **408**, 488-492.

Ichimura, Y., Imamura, Y., Emoto, K., Umeda, M., Noda, T. and Ohsumi, Y. (2004). In vivo and in vitro reconstitution of Atg8 conjugation essential for autophagy. *J. Biol. Chem.* **279**, 40584-40592.

Ichimura, Y., Kumanomidou, T., Sou, Y. S., Mizushima, T., Ezaki, J., Ueno, T., Kominami, E., Yamane, T., Tanaka, K. and Komatsu, M. (2008). Structural basis for sorting mechanism of p62 in selective autophagy. *J. Biol. Chem.* **283**, 22847-22857.

Kawamata, T., Kamada, Y., Kabeya, Y., Sekito, T. and Ohsumi, Y. (2008). Organization of the pre-autophagosomal structure responsible for autophagosome formation. *Mol. Biol. Cell* **19**, 2039-2050.

Kirisako, T., Baba, M., Ishihara, N., Miyazawa, K., Ohsumi, M., Yoshimori, T., Noda, T. and Ohsumi, Y. (1999). Formation process of autophagosome is traced with Apg8/Aut7p in yeast. *J. Cell Biol.* **147**, 435-446.

Kirisako, T., Ichimura, Y., Okada, H., Kabeya, Y., Mizushima, N., Yoshimori, T., Ohsumi, M., Takao, T., Noda, T. and Ohsumi, Y. (2000). The reversible modification regulates the membrane-binding state of Apg8/Aut7 essential for autophagy and the cytoplasm to vacuole targeting pathway. *J. Cell Biol.* **151**, 263-276.

Klionsky, D. J., Cregg, J. M., Dunn, W. A., Jr, Emr, S. D., Sakai, Y., Sandoval, I. V., Sibirny, A., Subramani, S., Thumm, M., Veenhuis, M. et al. (2003). A unified nomenclature for yeast autophagy-related genes. *Dev. Cell* **5**, 539-545.

Kuma, A., Mizushima, N., Ishihara, N. and Ohsumi, Y. (2002). Formation of the approximately 350-kDa Apg12-Apg5.Apg16 multimeric complex, mediated by Apg16 oligomerization, is essential for autophagy in yeast. *J. Biol. Chem.* **277**, 18619-18625.

Lang, T., Schaeffeler, E., Bernreuther, D., Bredschneider, M., Wolf, D. H. and Thumm, M. (1998). Aut2p and Aut7p, two novel microtubule-associated proteins are essential for delivery of autophagic vesicles to the vacuole. *EMBO J.* **17**, 3597-3607.

Legesse-Miller, A., Sagiv, Y., Glozman, R. and Elazar, Z. (2000). Aut7p, a soluble autophagic factor, participates in multiple membrane trafficking processes. *J. Biol. Chem.* **275**, 32966-32973.

Longtine, M. S., McKenzie, A., 3rd, Demarini, D. J., Shah, N. G., Wach, A., Brachat, A., Philippsen, P. and Pringle, J. R. (1998). Additional modules for versatile and economical PCR-based gene deletion and modification in Saccharomyces cerevisiae. *Yeast* **14**, 953-961.

Mizushima, N., Noda, T., Yoshimori, T., Tanaka, Y., Ishii, T., George, M. D., Klionsky, D. J., Ohsumi, M. and Ohsumi, Y. (1998). A protein conjugation system essential for autophagy. *Nature* **395**, 395-398.

Mukaiyama, H., Oku, M., Baba, M., Samizo, T., Hammond, A. T., Glick, B. S., Kato, N. and Sakai, Y. (2002). Paz2 and 13 other PAZ gene products regulate vacuolar engulfment of peroxisomes during micropexophagy. *Genes Cells* **7**, 75-90.

Mukaiyama, H., Baba, M., Osumi, M., Aoyagi, S., Kato, N., Ohsumi, Y. and Sakai, Y. (2004). Modification of a ubiquitin-like protein Paz2 conducted micropexophagy through formation of a novel membrane structure. *Mol. Biol. Cell* **15**, 58-70.

Nakatogawa, H., Ichimura, Y. and Ohsumi, Y. (2007). Atg8, a ubiquitin-like protein required for autophagosome formation, mediates membrane tethering and hemifusion. *Cell* **130**, 165-178.

Noda, N. N., Kumeta, H., Nakatogawa, H., Satoo, K., Adachi, W., Ishii, J., Fujioka, Y., Ohsumi, Y. and Inagaki, F. (2008). Structural basis of target recognition by Atg8/LC3 during selective autophagy. *Genes Cells* **13**, 1211-1218.

Oh-oka, K., Nakatogawa, H. and Ohsumi, Y. (2008). Physiological pH and acidic phospholipids contribute to substrate specificity in lipidation of Atg8. *J. Biol. Chem.* **283**, 21847-21852.

Sakai, Y., Kazarimoto, T. and Tani, Y. (1991). Transformation system for an asporogenous methylotrophic yeast, Candida boidinii: cloning of the orotidine-5′-phosphate decarboxylase gene (URA3), isolation of uracil auxotrophic mutants, and use of the mutants for integrative transformation. *J. Bacteriol.* **173**, 7458-7463.

Sakai, Y., Koller, A., Rangell, L. K., Keller, G. A. and Subramani, S. (1998). Peroxisome degradation by microautophagy in Pichia pastoris: identification of specific steps and morphological intermediates. *J. Cell Biol.* **141**, 625-636.

Sears, I. B., O'Connor, J., Rossanese, O. W. and Glick, B. S. (1998). A versatile set of vectors for constitutive and regulated gene expression in Pichia pastoris. *Yeast* **14**, 783-790.

van der Klei, I. J., Yurimoto, H., Sakai, Y. and Veenhuis, M. (2006). The significance of peroxisomes in methanol metabolism in methylotrophic yeast. *Biochim. Biophys. Acta* **1763**, 1453-1462.

Wang, L., Seeley, E. S., Wickner, W. and Merz, A. J. (2002). Vacuole fusion at a ring of vertex docking sites leaves membrane fragments within the organelle. *Cell* **108**, 357-369.

Wang, L., Merz, A. J., Collins, K. M. and Wickner, W. (2003). Hierarchy of protein assembly at the vertex ring domain for yeast vacuole docking and fusion. *J. Cell Biol.* **160**, 365-374.

Weisman, L. S. (2003). Yeast vacuole inheritance and dynamics. *Annu. Rev. Genet.* **37**, 435-460.

Wickner, W. and Haas, A. (2000). Yeast homotypic vacuole fusion: a window on organelle trafficking mechanisms. *Annu. Rev. Biochem.* **69**, 247-275.

Yamashita, S., Oku, M., Wasada, Y., Ano, Y. and Sakai, Y. (2006). PI4P-signaling pathway for the synthesis of a nascent membrane structure in selective autophagy. *J. Cell Biol.* **173**, 709-717.

Yamashita, S., Yurimoto, H., Murakami, D., Yoshikawa, M., Oku, M. and Sakai, Y. (2009). Lag-phase autophagy in the methylotrophic yeast Pichia pastoris. *Genes Cells* **14**, 861-870.

Table S1. Yeast strains used in this study

Strain	Genotype	Reference
P. pastoris		
PPY12	*arg4 his4*	Sakai *et al*. (1998)
NTP0101	PPY12 *atg1*::Zeo^r	This study
PPM5010	PPY12 *atg8*::Zeo^r	Mukaiyama *et al*.(2002)
PPM5011	PPM5010 *his4*::pHM104	Mukaiyama *et al*.(2002)
NTP0802	PPY12 *atg7*::Zeo^r	This study
NTP0803	NTP0802 *atg8*::pHM112	This study
NTP0804	NTP0803 *his4*::pHM104	This study
NTP0801	PPM5010 *his4*::pNT801	This study
PPM5016	PPM5010 *his4*::pHM106	Mukaiyama *et al*.(2002)
NTP0805	PPM5030 *his4*::pHM104	This study
PPM5017	PPM5010 *his4*::pHM110	Mukaiyama *et al*.(2002)
NTP0806	PPM5010 *his4*::pNT802	This study
NTP0807	PPM5010 *his4*::pNT803	This study
NTP0808	PPM5010 *his4*::pNT804	This study
NTP0809	PPM5010 *his4*::pNT805	This study
NTP0810	PPM5010 *his4*::pNT806	This study
NTP0811	PPM5010 *his4*::pNT807	This study
NTP0812	PPM5010 *his4*::pNT808	This study
NTP0813	NTP0803 *his4*::pNT802	This study
NTP0814	NTP0803 *his4*::pNT804	This study
NTP0815	NTP0803 *his4*::pNT806	This study
NTP0816	NTP0803 *his4*::pNT807	This study
NTP0817	NTP0803 *his4*::pNT809	This study
NTP0818	NTP0803 *his4*::pNT810	This study
NTP0819	NTP0803 *his4*::pNT811	This study
NTP0820	PPM5010 *arg4*::pSAP115	This study
NTP0821	PPM5010 *his4*::pNT812	This study
NTP0001	PPY12 *arg4*::pSAP500	This study
NTP0102	NTP0101 *arg4*::pSAP500	This study
NTP0822	PPM5010 *arg4*::pSAP500	This study
NTP0823	NTP0101 *atg8*::pHM112	This study
NTP0824	NTP0803 *his4*::pNT813	This study
NTP0825	NTP0803 *his4*::pNT814	This study
NTP0826	NTP0803 *his4*::pNT815	This study
NTP0827	PPM5010 *his4*::pNT816	This study
NTP0828	PPM5010 his4::pNT817	This study
NTP0829	NTP0828 his4::pNI005	This study
S. cerevisiae		
YMO100	W303-1A, *ADE2*	This study
YMO101	YMO100, *atg1*::*SpHIS5*	This study
YMO107	YMO100, *atg7*::*SpHIS5*	This study
YMO108	YMO100, *atg8*::*SpHIS5*	This study

Table S2. Primers used in this study

Desination	DNA Sequence
ATG8PromFw-EcoRI	5'-GGAATTCGGATCTAAGGTTACCGCTTTCGAC-3'
ATG8TFRv-XhoI	5'-CCGCTCGAGTTAAAACGTGTTTTCTCCGCTGTAAAG-3'
ATG8I32AFw	5'-GCGGACCGTATCCCCGTGGCTTGTGAGAAAGTGGAGAAG-3'
ATG8I32ARv	5'-CTTCTCCACTTTCTCACAAGCCACGGGGATACGGTCCGC-3'
ATG8K48AFw	5'-CCAGAGGTAGATAAGCGGGCTTACCTGGTTCCATGCGACC-3'
ATG8K48ARv	5'-GGTCGCATGGAACCAGGTAAGCCCGCTTATCTACCTCTGG-3'
ATG8L50AFw	5'-GGTAGATAAGCGGAAGTACGCTGTTCCATGCGACCTAACTG-3'
ATG8L50ARv	5'-CAGTTAGGTCGCATGGAACAGCGTACTTCCGCTTATCTACC-3'
ATG8V61AFw	5'-CTAACTGTGGGCCAGTTTGTGGCTGTTATCCGAAAGAGAATTAAG-3'
ATG8V61ARv	5'-CTTAATTCTCTTTCGGATAACAGCCACAAACTGGCCCACAGTTAGGA-3'
ATG8R65AFw	5'-GGGCCAGTTTGTGTACGTTATCGCTAAGAGAATTAAGATCCCATCTG-3'
ATG8R65ARv	5'-CAGATGGGATCTTAATTCTCTTAGCGATAACGTACACAAACTGGCCC-3'
ATG8F104AFw	5'-AGAACATAAAGATGAGGACGGGGCTTTGTACGTTCTTTACAGCGGAG-3'
ATG8F104ARv	5'-CTCCGCTGTAAAGAACGTACAAAGCCCCGTCCTCATCTTTATGTTCT-3'
ATG8Y106AFw	5'-GATGAGGACGGGTTTTTGGCTGTTCTTTACAGCGGAGAAAAC-3'
ATG8Y106ARv	5'-GTTTTCTCCGCTGTAAAGAACAGCCAAAAACCCGTCCTCATC-3'
HAFw-EcoRI	5'-GGAATTCATGTCTAGATCTATCTTTTACCCATAC-3'
ATG8FGRv-XhoI	5'-CCGCTCGAGTTATCCAAACGTGTTTTCTCCGCTGTA-3'
ATG8A9Rv-XhoI	5'-CCGCTCGAGTTAAGCAGCAGCAGCAGCAGCAGCAGCTCCAAACGTGTTTTCTCCGCTGTA-3'
CFPFw-PstI	5'-AACTGCAGATGGTGAGCAAGGGCGAGGAGC-3'
CFPRv-PstI	5'-AACTGCAGCTTGTACAGCTCGTCCATGCC-3'
YFPFw-HindIII	5'-CCCAAGCTTGTGAGCAAGGGCGAGGAG-3'
YFPRv-HindIII	5'-CCCAAGCTTTTACTTGTACAGCTCGTCCAT-3'
ATG17UPFw-BamHI	5'-CGGGATCCTCATGTAGACCTACAGAGGCCATG-3'
ATG17Rv-XhoI	5'-CCGCTCGAGCTTCCTTCCCAGTATTGCAATGCGT-3'

Table S3. Plasmids used in this study

Desination	Discription	Reference
pHM104	HA-PpATG8 HIS4	Mukaiyama *et al.*(2002)
pHM106	HA-PpATG8FG HIS4	Mukaiyama *et al.*(2002)
pHM110	HA-PpATG8G116A HIS4	Mukaiyama *et al.*(2002)
pPM112	ΔPpatg8	Mukaiyama *et al.*(2004)
pSAP115	YFP-PpATG8 ARG4	Mukaiyama *et al.*(2004)
pSAP500	SK-ARG4 ARG4	Ano *et al.*(2004)
pNT801	HA-PpATG8FT HIS4	This study
pNT802	HA-PpATG8I32A HIS4	This study
pNT803	HA-PpATG8K48A HIS4	This study
pNT804	HA-PpATG8L50A HIS4	This study
pNT805	HA-PpATG8V61A HIS4	This study
pNT806	HA-PpATG8R65A HIS4	This study
pNT807	HA-PpATG8F104A HIS4	This study
pNT808	HA-PpATG8Y106A HIS4	This study
pNT809	P_{GAPDH}HA-PpATG8FG HIS4	This study
pNT810	P_{GAPDH}HA-PpATG8FGR65A HIS4	This study
pNT811	P_{GAPDH}HA-PpATG8FGF104A HIS4	This study
pNT812	P_{ATG8}YFP-PpATG8 HIS4	This study
pNT813	P_{ATG8}YFP-PpATG8R65A HIS4	This study
pNT814	P_{ATG8}YFP-PpATG8F104A HIS4	This study
pNT815	P_{ATG8}YFP-PpATG8G116A HIS4	This study
pNT816	HA-PpATG8A9 HIS4	This study
pNT817	CFP-PpATG8 HIS4	This study
pNT204	PIB1ARG4	This study
pNT205	YFP-PIB1ARG4	This study
pNI005	P_{ATG17}PpATG17-YFP ARG4	This study